# Using *Ab Initio* Calculations in the Calphad Environment

**B.P. Burton[1], N. Dupin[2], S. G. Fries[3], G. Grimvall[4], A. Fernández Guillermet[5], P. Miodownik[6], W. Alan Oates[7], and V. Vinograd[8]**

[1]A226/223 NIST, Gaithersburg MD 20899-8520 USA; benjamin.burton@nist.gov [2]Calcul Thermodynamique, 3, rue de l'avenir, 63670 Orcet, France; dupin@ltpcm.inpg.fr [3]ACCESS e.V., RWTH-Aachen, Intzestr. 5, D-52072 Aachen, Germany; sufries@aldix.mpi-stuttgart.mpg.de [4]Department of Theoretical Physics, The Royal Institute of Technology, S-100 44 Stockholm, Sweden; grimvall@theophys.kth.se [5]Consejo Nacional de Investigaciones Cientificas y Tecnicas Centro Atomico Bariloche, 8400 Bariloche, Argentina; afg@cab.cnea.gov.ar [6]ThermoTech, Surrey Technology Centre, Guildford. UK; p.miodownik@btinternet.com [7]Science Research Institute, University of Salford, Salford M5 4WT, UK; ctguest@chorus.net [8]Institut fur Mineralogie, Universitat Münster Correnssstr. 24, D-48149 Münster Germany; vinogra@uni-muenster.de

Published in Zeitschrift fur Metallkunde **92,** 514- (2001)

## Abstract

Methods for applying first principles (FP) calculations to CALPHAD modeling, are discussed, with emphasis on easily calculated quantities that can be used to estimate input parameters for CALPHAD optimizations. Estimations of vibrational entropies, and melting points, from chemical systematics of measured elastic constants, or via semiempirical methods based on FP-calculations are reviewed. Some strategies for including higher-order (clusters larger than pairs) short range order correlations in CALPHAD calculations are considered.

## 1 Introduction

Previous Ringberg working groups have discussed possible applications of first principles (FP) calculations to CALPHAD modeling, and have considered the problems arising from neglect of short range order (SRO) in CALPHAD Gibbs energy models [1]. Particular attention has been directed towards understanding how mechanical instabilities account for the large differences between FP-calculated lattice stabilities and those derived from extrapolations of CALPHAD Gibbs energy models[2, 3]. Related issues are addressed in this report with emphasis on insulating materials. Also, strategies for estimating vibrational entropies and melting points from FP-calculations or chemical systematics are discussed. Some strategies for including SRO (beyond pair correlations) in CALPHAD calculations are discussed in the final section. Sections 2 and 5 are con-

cerned with using FP electronic structure calculations to obtain composition dependent thermodynamic functions and physical properties. Sections 3 and 4 (primarily) deal with stoichiometric compounds, and semiempirical chemical systematics.

# 2 Uses of Electronic Structure Calculations in support of CALPHAD Optimizations

At present, it seems impractical to incorporate complete first principles (FP) phase diagram (FPPD) calculations into the CALPHAD method, however, certain elements of the FPPD technique can easily be used to augment, or complement, CALPHAD optimizations. In particular, electronic structure codes based on density functional theory, in the local density approximation (LDA); the Vienna Abinitio Simulation Package; VASP [4] are becoming sufficiently user friendly that CALPHAD practitioners may find them useful for generating initial estimates of various physical properties. For example, VASP calculations of such quantities as: equations of state (EOS), molar volumes ($V$), and bulk moduli ($B$, $B'$) are trivial; as are calculations of formation energies ($\Delta E_f$) for pure compounds with fewer than about 80 atoms per unit cell. More difficult to calculate, but not excessively so, are elastic constants, $c_{ij}$ and force-constant matricies, for stability analyses. In addition, the VASP package can perform finite temperature calculations from which one might, for example, calculate vibrational entropies.

## 2.1 Using EOS Data

### 2.1.1 Bulk Moduli and Equilibrium Volumes

VASP EOS ($E(V)$) calculations were performed for the B1, NaCl-structure, carbides: VC, TiC, NbC, and ZrC, and some results are listed in Table 1 and plotted in Fig. 1. Fits to the $E(V)$ data, with second, third, and fourth order polynomials, were considered. Results for $B$ and $B'$:

$$B = V\left[\frac{d^2E(V)}{dV^2}\right]_{V_0} \tag{1}$$

$$B' = -\left(1 + \frac{V^2}{B}\left[\frac{dE(V)}{dV}\right]_{V_0}\right) \tag{2}$$

(where V is molar volume and $V_0$ is the equilibrium molar volume at 0K) are in good agreement with previous calculations [5] that were mostly done with full potential linear muffin tin orbital (FPLMTO) code. For EOS calculations of this sort, however, the VASP program is generally preferable because it performs ionic relaxations routinely, whereas the FPLMTO and other LMTO codes do not. This makes no difference for B1 structure compounds, but is important for lower symmetry phases.

Table 1: VASP-calculated equation of state related quantities

| System | Polynomial Fit Order | $V_{Exp}/Atom$ ($\AA^3$) | $V_0/Atom$ ($\AA^3$) | $E_0/Atom$ ($eV$) | $B$ GPa | $B'$ GPa |
|---|---|---|---|---|---|---|
| VC | 2 | 8.9983 | 8.615 | -10.543 | 2.09 | |
| TiC | 2 | 10.061 | 9.741 | -10.246 | 1.72 | |
| NbC | 2 | 11.164 | 11.068 | -11.146 | 1.99 | |
| ZrC | 2 | 12.942 | 12.705 | -10.540 | 1.49 | |
| VC | 3 | | 8.613 | -10.543 | 2.16 | 3.98 |
| TiC | 3 | | 9.733 | -10.246 | 1.75 | 3.79 |
| NbC | 3 | | 11.065 | -11.146 | 2.05 | 4.37 |
| ZrC | 3 | | 12.698 | -10.540 | 1.52 | 3.96 |
| VC | 4 | | 8.613 | -10.543 | 2.16 | 3.91 |
| TiC | 4 | | 9.733 | -10.246 | 1.75 | 3.89 |
| NbC | 4 | | 11.065 | -11.146 | 2.05 | 4.13 |
| ZrC | 4 | | 12.698 | -10.540 | 1.51 | 4.06 |

The VASP calculations yield typical LDA results for $V_0$ (Fig. 1); i.e. LDA systematically underestimates $V_0$ such that $V_{Calc} \approx 0.96 V_{Exp}$. The dashed line in Fig. 1 indicates where the $V_{Calc}$ results would plot if they agreed perfectly with experiment, and the dotted line indicates a deviation of $-4$ % from perfect agreement. As discussed in Section 2 the $B$ and $B'$ parameters can be used to estimate Debye temperatures.

### 2.1.2 Estimating $\Delta E_{elastic}$ from EOS Calculations

Ferreira et al. [6], approximated the elastic contribution to the excess enthalpy of mixing, $\Delta H_{elastic}$, with their $\epsilon - G$ approximation (in which $\epsilon$ is a short range chemical interaction and $G$ is a long-range elastic interaction). The advantage of this approach is that $\Delta H_{elastic}$, which is approximated as equal to $\Delta E_{elastic}$, can be estimated from the EOS of two pure end member phases.

The procedure is:

- Calculate EOS for the end members, TiC and ZrC in this case (Fig. 2).
- Transform, $E = E(V)$, into $E = E(X)$ via the approximation that, $V$ is linear in bulk composition, $X = X_{ZrC}$, such that $(V = a + bX)$; this is probably a good approximation for the *random* alloy.
- Approximate $\Delta E(X)$ as a linear combination of partials from the two end member EOS (Fig. 3).

The final step can be written formally as:

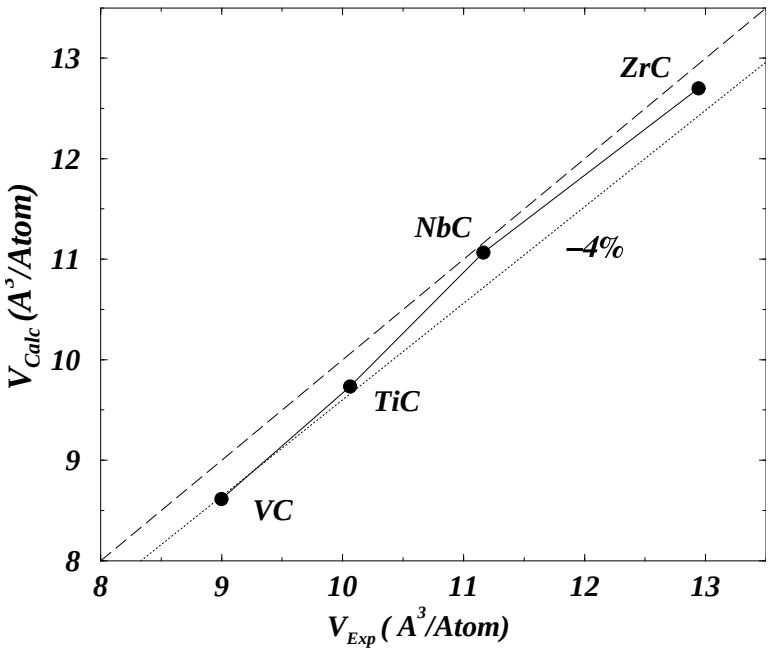


Figure 1: Comparison of experimental and VASP calculated volumes for some B1 carbides.

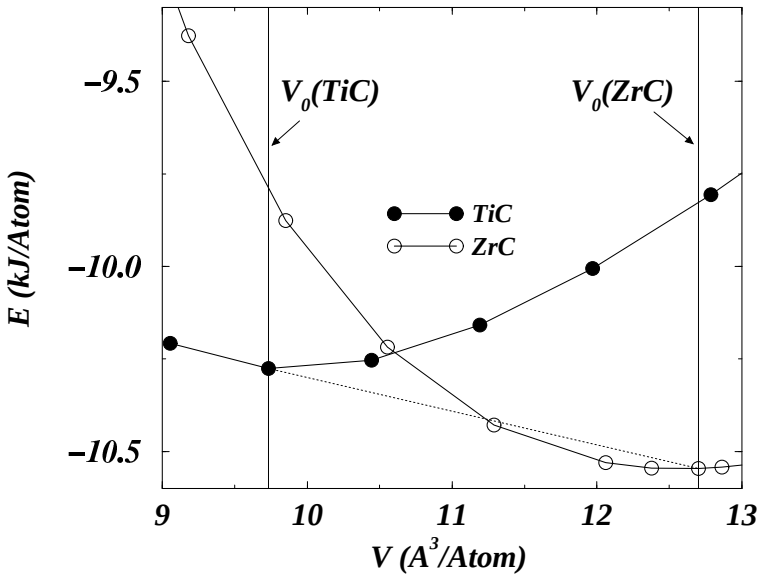


Figure 2: Equations of State for TiC and ZrC plotted as functions of volume, which can be converted to functions of bulk composition ($X_{Zr}$) via the approximation $V = 9.73 + 2.97X_{Zr}$.

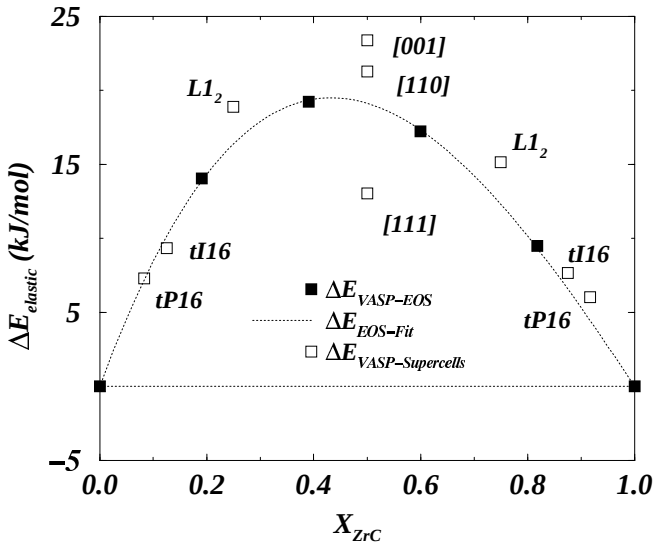


Figure 3: The approximate curve for $E_{elastic}$.

$$\Delta E_{elastic}(X) = (1 - X)E_{TiC}(X) \; + \; XE_{ZrC}(X) \tag{3}$$

Where $E_{TiC}(X)$ is the energy of pure TiC evaluated at the value of $V$ corresponding to value of X specified by the solid square, and similarly for $E_{ZrC}(X)$ (i.e. to calculate one value of $\Delta E_{elastic}$, corresponding to a single solid square: calculate $V_{TiC}$ and $V_{ZrC}$ from $V = 9.73{+}2.97X$; evaluate $E_{TiC}(V)$ and $E_{ZrC}(V)$ at this value of $V$; plug $E_{TiC}(V)$ and $E_{ZrC}(V)$ into Equation 3.)

Fig. 3 shows the approximation based on VASP EOS (solid squares plus the dotted curve fit to them). In addition, nine VASP supercell calculations are indicated by the open squares which are formation energies for selected ordered compounds: $L1_2$; [001]; [110]; and [111] superlattices; $tI16$ and $tP16$ (tetragonal 16 atom cells that are doubled NaCl cells). The rough coincidence between the envelope of values defined by the supercell formation energies and the $\Delta E_{elastic}(X)$ curve suggests that for the $Ti_{1-x}Zr_xC$ system, $\Delta H^{XS} \approx \Delta E_{elastic}$ is a reasonable approximation. Note that supercell volumes, Fig. 4 deviate little from Vegards' law ($V$ linear in X), which also suggests that the main source of nonideal mixing in $Ti_{1-x}Zr_xC$ is a size effect; and therefore $\Delta E_{elastic}(X) \approx \Delta H^{XS}$. Note that $\Delta E_{elastic}(X)$ has the appropriate asymmetry; i.e. it requires more energy to insert larger Zr atoms in TiC-rich solutions than to insert smaller Ti atoms in ZrC-rich solutions. That the [111] supercell

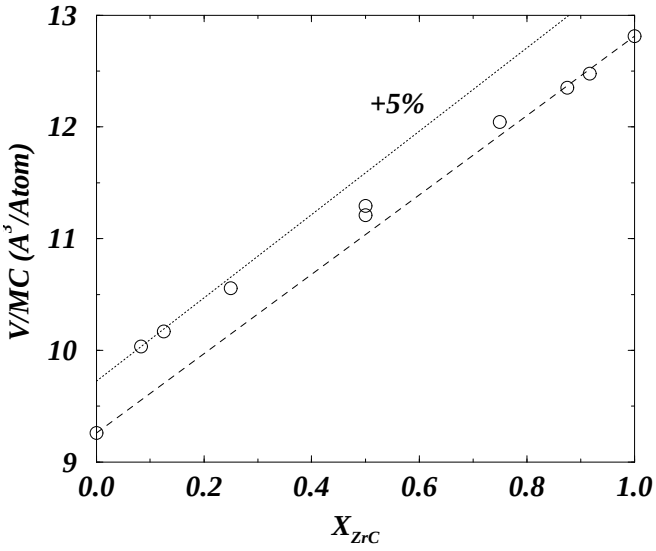


Figure 4: Calculated supercell volumes: Dashed line is Vegards' Law; Dotted line indicates a five percent deviation from Vegards' law.

formation energy, $\Delta E_{[111]}$, is only about 70% of $\Delta E_{elastic}(X = 1/2)$ suggests that SRO related to this structure will reduce $\Delta H^{XS}$, relative to $\Delta E_{elastic}(X)$, in the neighborhood of $X \approx 0.5$. Therefore, the approximation $\Delta H^{XS} \approx \Delta E_{elastic}$ may be a good starting point for an unknown system, but it should be treated as an upper bound, because SRO may significantly reduce $\Delta H^{XS}$.

## 2.2 "Charged" Reference States in CEF Models

### 2.2.1 Formation Energies and Band-Filling Energy

Compound energy formalism (CEF) [7] often have fictive end members to which a formal charge is attributed. For example, in the perovskite structure quasi-binary system $PbNbO_3$-$PbMgO_3$, only $Pb(Mg_{1/3},Nb_{2/3})O_3$ occurs in nature, and if one insists on formal valences: $Pb^{+2}$, $Nb^{+5}$, $Mg^{+2}$, $O^{-2}$, the end members would be $PbNbO_3^{+1}$ and $PbMgO_3^{-2}$. Alternatively, one can assume that valences change to maintain global electrical neutrality. The former approach is fundamentally unphysical, and therefore can not be modeled directly with FP-calculations, but the latter often can. In $PbNbO_3$-$PbMgO_3$ (Fig. 5), one can calculate formation energies for $PbNbO_3$, $PbMgO_3$, and a variety of ordered supercells of intermediate composition (these $\Delta E_f$ values are the formation energies that one may use to fit a Cluster Expansion Hamiltonian, as discussed in

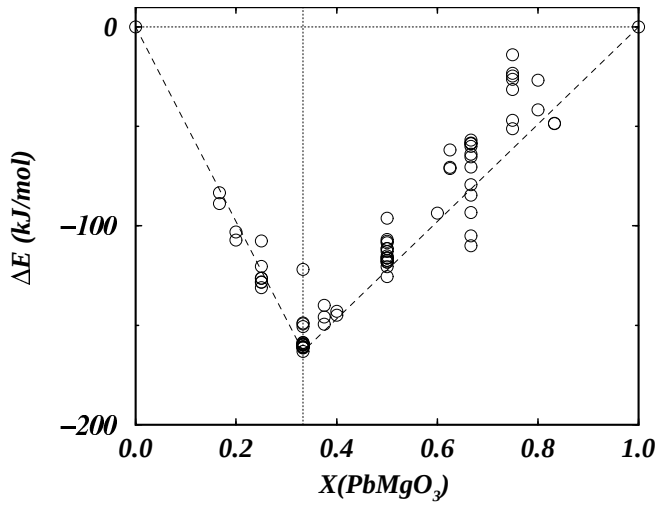


Figure 5: VASP calculations of formation energies in the quasibinary system $PbNbO_3$-$PbMgO_3$; dashed line is to emphasize the approximately linear trends of $\Delta E_f(X)$.

Section 5. The electronic structure calculation begins with neutral atoms, and adjusts the electron density to obtain a minimum energy configuration, but that configuration need not respect formal valences; electrical neutrality is a more important physical constraint. Fictive neutral end members are typically high in energy, and the energies of fictive compounds, between them and the minimum (where nominal valences apply) follow two approximately linear trends (Fig. 5, $Pb(Mg_xNb_{1-x})O_3$; Fig. 6, $[Na_{1-x}Bi_x]TiO_3$). The approximate linearities of these trends are consequences of the linear composition-dependencies of the concentrations of holes [$1/3 < X(PbMgO_3) \leq 1$], or electrons promoted to the conduction band [$0 < X(PbMgO_3) \leq 1/3$]. Because the form of the band changes slowly with composition, and little with ordering, this *nonconfigurational* band-filling (BF) energy ($E_{BF}$) is approximately the density of holes, or promoted electrons, times the energy per hole ($e^-$ promoted).

A naive attempt was made to calculate $E_{BF}$ for a series of [001] superstructures with the following approximations.

1) For $1/3 < X(PbMgO_3) \leq 1$, calculating the energy associated with depleting the band:

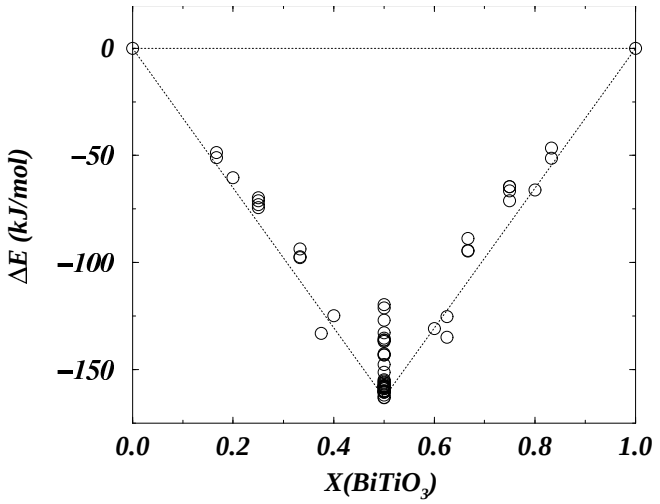


Figure 6: VASP calculations of formation energies in the quasibinary system $NaTiO_3$-$BiTiO_3$; dashed line is to emphasize the approximately linear trends of $\Delta E_f(X)$.

$$E_{BF} \approx \frac{1}{2}\int_{E-Fermi}^{Top\ of\ Band} E \cdot D(e^-)dE \tag{4}$$

where $D(e^-)$ is the electronic density of states.

For $0 < X(\mathrm{PbMgO_3}) \leq 1/3$, calculating the energy associated with promoting electrons into the conduction band:

$$E_{BF} \approx \frac{1}{2}\int_{Bottom\ of\ Conduction\ Band}^{E-Fermi} E \cdot D(e^-)dE \tag{5}$$

Factors of 1/2 are present to avoid double counting.

Results of this calculation are plotted in Fig. 7, along with the formation energies from Fig. 5. Apparently, these naive approximations for $E_{BF}(X)$ fail, because they yield corrections that are more negative than the formation energies, by a factor of about two. Qualitatively however, linear trends for $E_{BF}(X)$ are clearly apparent. It follows that, when fitting the energetics of a quasibinary system with fictive end members (that have nonstandard ionic valences) one

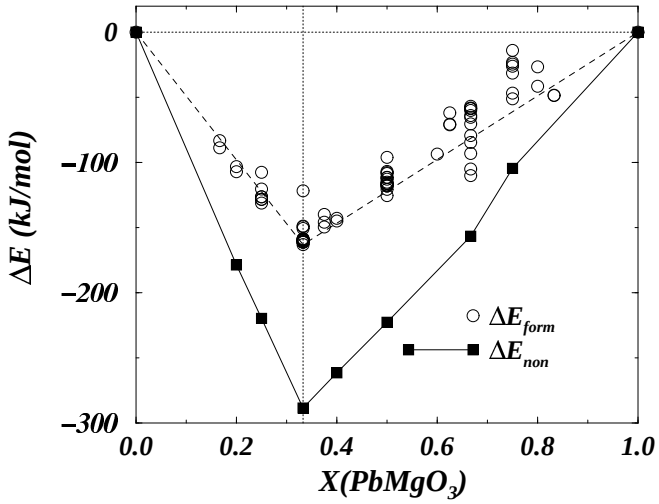


Figure 7: Calculations of the band-filling energy associated with depleting a band $0 < X(\mathrm{PbMgO_3}) \leq 1/3$, or forcing electrons into the conduction band $1/3 < X(\mathrm{PbMgO_3}) \leq 1$. Supercell formation energies are plotted for comparison.

should include two or more nonconfigurational $E_{BF}(X)$ terms that are linear in composition.

Therefore, it may sometimes be possible to abandon the fundamentally unphysical construct of charged reference states that occur in CEF, in favor of more physical end members with formation energies that can be calculated from first principles.

### 2.2.2 Mechanical Stability

Fictive end members are, of course, subject to the same mechanical stability issues that arise with lattice stabilities for various metals; e.g. body centered cubic (bcc) Al. Stability analyses of the $Pm\bar{3}m$ perovskite structure phases $PbMgO_3$ and $PbNbO_3$, were performed by using VASP calculations to obtain force-constant matrices, and then performing eigenvalue analyses. These calculations clearly revealed mechanical (tetragonal ferroelectric) instabilities of the sort that are observed in $PbTiO_3$ [8]. Instabilities of this type can involve substantial, or trivial, energies depending on particular composition (Fig. 8 and 9). For example:

$$\Delta E(PbMgO_3) = E_{tetragonal} - E_{cubic} \approx -70\ kJ/mol$$
$$\Delta E(PbNbO_3) = E_{tetragonal} - E_{cubic} \approx -0.1\ kJ/mol$$

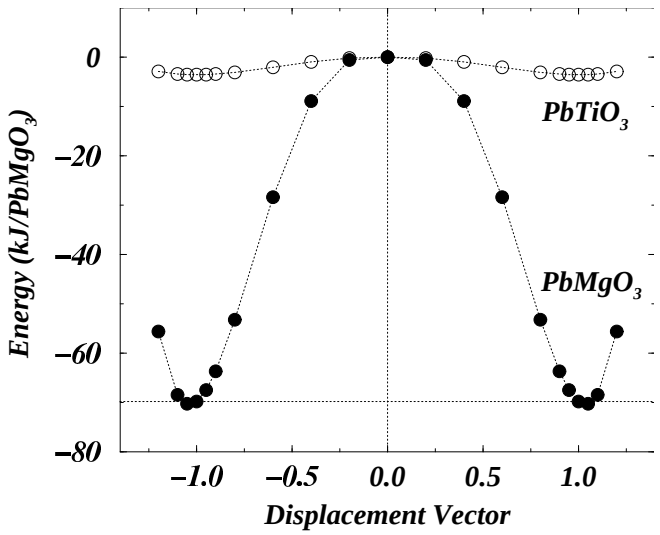


Figure 8: VASP calculation of the double well ferroelectric instability in $PbMgO_3$ compared to that in $PbTiO_3$.

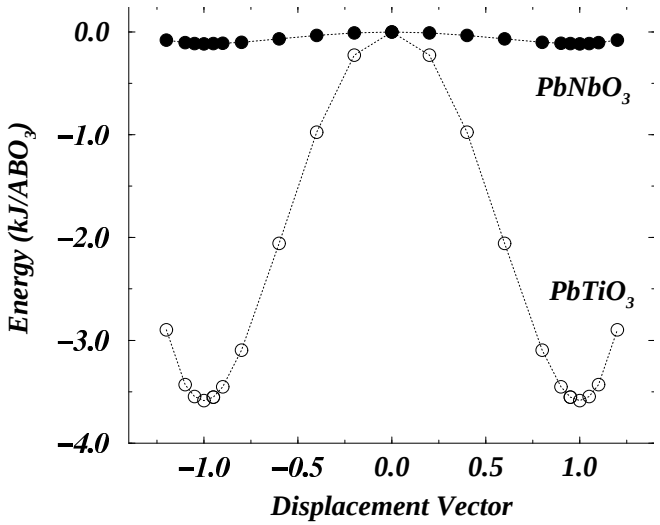


Figure 9: VASP calculation of the double well ferroelectric instability in $PbNbO_3$ compared to that in $PbTiO_3$. Note the order of magnitude difference between the energy scales of this Figure and the previous one.

# 3 Calculation of Vibrational Entropy and Elastic Properties

## 3.1 Basic Concepts and Definitions

The temperature dependent part of the Gibbs energy of an element or a stoichiometric compound is usually dominated by the lattice vibrations, which may be described by a properly defined Debye temperature, $\Theta$. Following [9] we shall use an "entropy Debye temperature", $\Theta_S$. It is obtained from the $\Theta_S(T)$ function that reproduces the experimental vibrational entropy per atom of the compound, $S_{vib}$, if $\Theta_S$ is inserted in the expression for entropy $S_D$, in the Debye model,

$$S_{vib}(T) = S_D\left[\frac{\Theta_S(T)}{T}\right] \tag{6}$$

At low temperatures ($T << \Theta_S$), $\Theta_S(T)$ varies with $T$ because the true vibrational spectrum is not of Debye form, and at high temperatures ($T > \Theta_S$) it shows a smooth decrease with increasing $T$, caused by anharmonic softening of the lattice vibrations. To obtain stable values for $\Theta_S$, we evaluated it at $T \approx \Theta_S$. At $T \geq \frac{\Theta_S}{2}$, $\Theta_S$ essentially measures a logarithmic average of the phonon frequencies, and in that particular average, the masses separate from the interatomic forces [10]. Therefore one can define a quantity $k_S$, with the dimension of a force constant (i.e. force per length), by

$$\Theta_S = \frac{h}{2\pi k}\sqrt{\frac{k_S}{M_{eff}}} \tag{7}$$

Here $M_{eff}$ is a "effective mass" defined as the logarithmic average of the atomic masses, $k$ is Boltzmanns' constant and $h$ is Plancks' constant. The quantity $k_S$, which contains information about the strength of the average interatomic forces in the compound, has been referred to as "effective force constant".

Other $k_i$ quantities with the dimension of a force constant have been introduced by Fernández *et al.* [11]. The quantity $k_B$ is defined in terms of the bulk modulus ($B$) and the volume per atom of the compound, $V$, as follows

$$k_B = BV^{1/3} \tag{8}$$

As seen in Section 1, $B$ and $V$ may be calculated *ab initio* when experiments are missing or impossible.

Fig. 10 (a), (b) and (c) are plots of experimental values of $B$, $V$ and $k_B$, versus group number (GN) in the periodic table, for several elements. These characteristic variations of cohesive properties across the periodic table have

been used to estimate unknown values and to judge theoretical predictions. In what follows we will consider correlations between $k_B$ and two kinds of Debye temperatures.

## 3.2 Systematics and Correlations for Debye Temperatures

Moruzzi *et al.* [12] proposed a semi-empirical equation for estimating the low-temperature Debye temperature $\Theta_D$ of elements from information obtained in ab initio calculations (*i. e. V, B* ) and the atomic mass ($M$), viz.,

$$\Theta_D = a\sqrt{\frac{k_B}{M}} \tag{9}$$

where $a$ is an empirical constant [12].

The purpose of this section is to establish a new correlation with $k_B$ which allows estimations of $\Theta_S$ for both elements and compounds. The experimental relation between $\Theta_D$ and $a\sqrt{k_B/M}$ for various elements is shown in Fig. 11a and 11b. Dashed lines represent the relation proposed by Moruzzi *et al.*; however, recent theoretical work [13] casts doubt on the use of such empirical correlation methods.

### 3.2.1 Analysis of $\Theta_S$ Data

In Fig. 11b, we plot $\Theta_S$ temperatures obtained from experimental determinations of vibrational entropies [14] versus experimental values for the quantity $\sqrt{k_B/M}$, for several elements. The symbols in Fig. 11a represent the $\Theta_D$ values for the same elements. The solid lines in these graphics represent the expression proposed by Moruzzi *et al.* [12] to predict $\Theta_D$ (Equation 9). The scatter of the $\Theta_S$ values is considerably less than that of the $\Theta_D$ values. In addition, we find that Equation 9 accounts remarkably well for the experimental $\Theta_S$ temperature whereas agreement with $\Theta_D$ could be improved by increasing the empirical constant, $a$; Note that $\Theta_S$ and $\Theta_D$ values for Be are significantly larger than those predicted by a linear extrapolation of the data. The anomalous behavior of Be is related to its unusal elastic properties, with a Poisson's constant close to zero that makes the shear modulus significantly larger than the bulk modulus [14].

### 3.2.2 Using *Ab Initio* Results

Fig. 12a is a plot of $\sqrt{k_B/M}$ versus number of valence electrons per atom, $n_e$, that we constructed with *ab initio* $B$ and $V$ values from Nguyen-Manh and Pettifor [15] for the transition metal aluminides ScAl, TiAl, CrAl, FeAl, CoAl, NiAl, YAl, ZrAl, MoAl, TcAl, RuAl, RhAl, PdAl and AgAl. Fig. 12b is a plot of $B$ as a function of $n_e$. We expect a similar trend for $\Theta_S$.

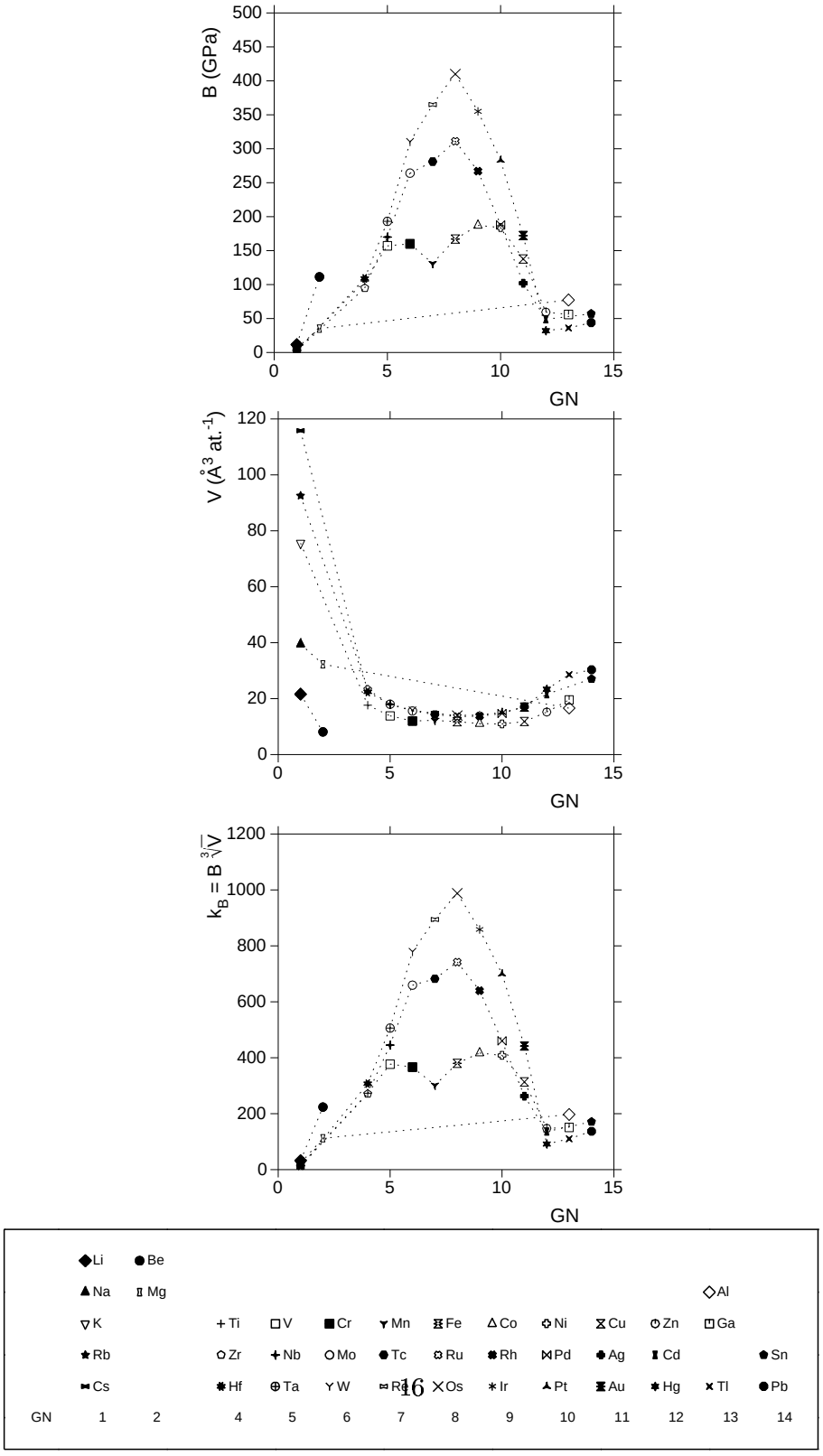


Figure 10: Experimental values of $B$ (a), $V$ (b) and $k_B$ (c) versus position in the periodic table

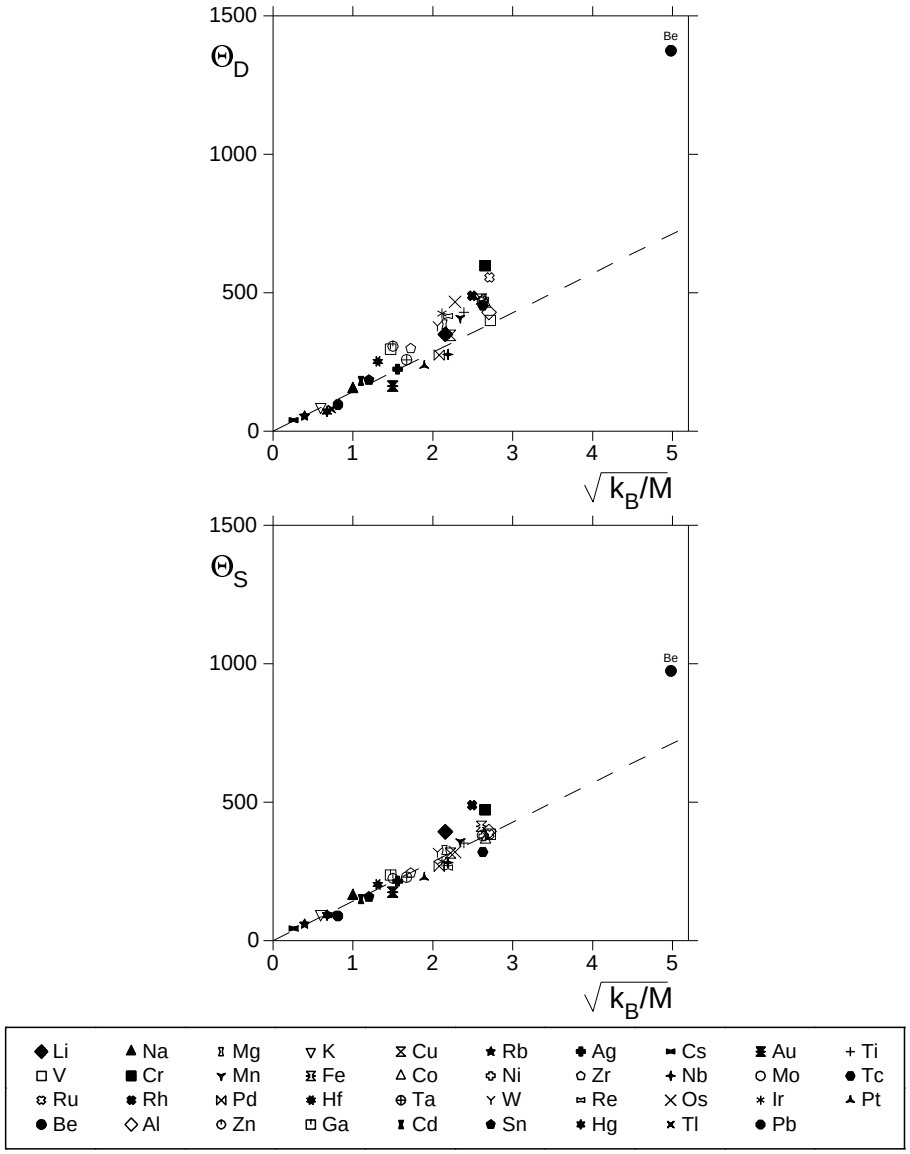


Figure 11: Experimental values of $\Theta_D$ (a) and $\Theta_S$ (b) versus $\sqrt{k_B/M}$. Dashed lines indicate the value predicted by Moruzzi *et al.*

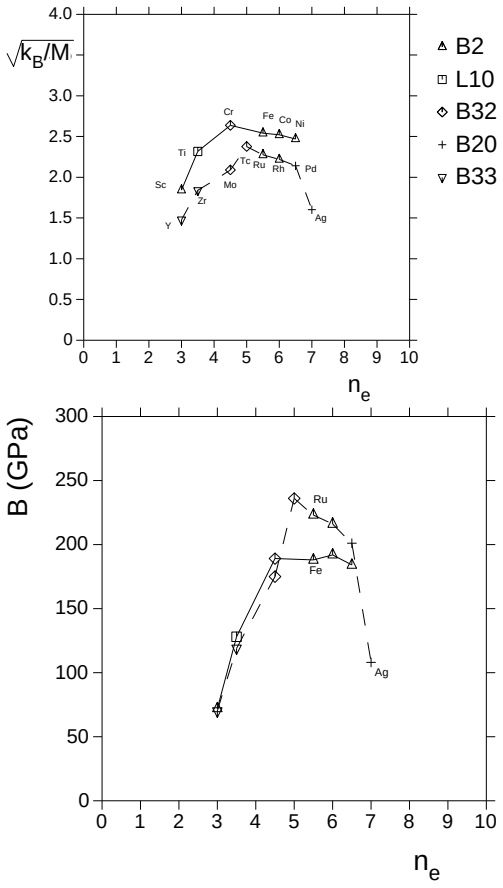


Figure 12: (a) $\sqrt{k_B/M}$ versus $n_e$; (b) $B$ versus $n_e$. Values obtained by us for the transition metal aluminides ScAl, TiAl, CrAl, FeAl, CoAl, NiAl, YAl, ZrAl, MoAl, TcAl, RuAl, RhAl, PdAl and AgAl, using the *ab initio* $B$ and $V$ results [15]

# 4 Using Elastic Properties to Establish Stabilities of Intermetallic Compounds

An important feature of the CALPHAD method is the characterization of *metastable*, or fictive *unstable*, intermetallic compounds that are sometimes called counter-phases. For example, there is no known FeC phase, but one needs an enthalpy of formation $\Delta H_f$ for FeC in the NaCl (B1) structure to model solid solutions of TiC with some Fe substituting for Ti. Often, thermodynamic functions and physical properties of counter-phases are estimated by extrapolation or interpolation of experimental data for isostructural phases. Alternatively, first principles (FP) calculations can be used; e.g. one can easily calculate the $\Delta E_f$ for FeC in the B1 structure (relative to bcc Fe and Graphite) and make the approximation $\Delta E_f \approx \Delta H_f$. Computational studies of pure elements have demonstrated, however, [16, 17, 18] that counter-phases may be *mechanically unstable*, and their FP-values for $\Delta E_f$ may be substantially higher than those obtained by CALPHAD extrapolation. Therefore, mechanical stability analysis must become a routine step in the use of FP calculations for estimating counter-phase energetics or physical properties (section 2.2.2: Mechanical Stability).

Stability criteria, with respect to elastic deformations, vary in complexity with crystal symmetry. In cubic structures (the following discussion is restricted to cubic structures) the criterion is:

$$(c_{11} - c_{12})/2 \geq 0 \tag{10}$$

Note that temperature dependencies of elastic constants are ignored, because of the scarcity of data, but a rigorous treatment would include them ( e.g. [19] for $Ni_3Al$).

## 4.1 Relationships Between Elastic Parameters

The stability criterion in Eq. 10 only requires two constants, $c_{11}$ and $c_{12}$, as does the the bulk modulus $B$ (Eq. 1). However the degree of anisotropy ($A$) is given by the ratio of the two shear moduli ($G/C'$) where $G$ is the modulus corresponding to shear on (100) planes in the [010] direction and $C'$ is the modulus corresponding to a shear on (110) planes in the [110] direction [14]:

$$B = (c_{11} + 2c_{12})/3 \tag{11}$$

$$C' = (c_{11} - c_{12})/2 \tag{12}$$

$$G_{100} = c_{44} \tag{13}$$

The degree of anisotropy is:

$$A = 2c_{44}/(c_{11} - c_{12}) \tag{14}$$

which requires a value for $c_{44}$. To obtain a correlation between macroscopic elastic properties and certain thermodynamic functions, it is useful to see how single crystal constants are related to $B$, $C'$, $G$, and Poisson's Ratio ($\nu$) in (quasi-) isotropic polycrystalline materials. A procedure devised by Hill [20] allows the effective engineering shear modulus $G$ to be calculated for such materials, despite the presence of anisotropy in single crystals ($A \neq 1$), and its absence in polycrystalline aggregates. One averages the values that are obtained when it is assumed that both strain and stress are uniform throughout the aggregate:

$$G_{average} = (G_V + G_R)/2 \tag{15}$$

where $G_V$ and $G_R$ stand for the values calculated by Voigt and Reuss, respectively, [20] and are:

$$G_R = 5c_{44}(c_{11} - c_{12})/[4c_{44} + 3(c_{11} - c_{12})] \tag{16}$$

$$G_V = (c_{11} - c_{12} + 3c_{44})/5 \tag{17}$$

The value of $B$ is independent of orientation, so the standard relationship between $G$ and $B$ can then be used to calculate a value of $\nu$ for such a quasi-isotropic polycrystalline aggregate [21]:

$$\nu = \frac{3B - 2G}{2(3B + G)} \tag{18}$$

Differences between $\nu_{100}$ and $\nu$, as calculated via Voigt-Reuss averaging, arises from differences in the the Anisotropy constant $A$. Youngs' modulus ($E$) can be derived from a combination of $\nu$ and $B$ or $G$ and $B$:

$$E = 3B(1 - 2\nu) \tag{19}$$

Such relationships are particularly useful for extrapolating variations in elastic properties from stable to metastable isostructural phases. Ideally a combination of different extrapolations should be used to obtain self-consistent results that give some indication of the mechanical stabilities, or instabilities, of metastable phases.

Unmeasured, values of some single crystal elastic constants may be derived by combining various forms of data. Values of $C'$ for 3d aluminides [15][a, b] and values of $B$ may be combined via Eq. 11 and 12 to extract $c_{11}$ and $c_{12}$. An advantage of this route is that $B$ does not vary much for close-packed structures ( See Fig 8 of [21] drawn from [22] or Table 2 of [23]), even when there is a substantial mechanical instability [18]. The data for Al-V in Table 2 were obtained by combining information from [15, 24]. Approximating single crystal elastic constants from the macroscopic elastic parameters, $E$, $G$, $B$ and $\nu$, leads to systematic errors because one always obtains $A = 1$, which implies an isotropic or quasi-isotropic material. When single crystal elastic constants have not been measured, however, this approach may give reasonable estimates.

Table 2: Calculated Elastic Properties of Some B2 Transitions Metal Compounds

| System | $c_{11}$ | $c_{12}$ | $c_{44}$ | $C'$ | $A$ | $B$ | $\nu_{100}$ | REF |
|---|---|---|---|---|---|---|---|---|
| Sc-Al | 90 | 63 | 98 | 14 | 7.26 | 72 | 0.41 | [15] $^{(b)}$ |
| Ti-Al | 85 | 149 | 82 | -32 | -2.56 | 128 | 0.64 | [15] $^{(a)}$ |
| V-Al | 23 | 227 | 73 | -102 | -0.72 | 159 | 0.91 | [15] $^{(a)}$ |
| Nb-Al | 1 | 227 | 38 | -113 | -0.34 | 152 | 1.00 | [15] $^{(a)}$ |
| Fe-Al | 292 | 136 | 166 | 78 | 2.13 | 188 | 0.32 | [15] $^{(b)}$ |
| Co-Al | 325 | 125 | 161 | 100 | 1.61 | 192 | 0.28 | [15] $^{(b)}$ |
| Ni-Al | 239 | 157 | 131 | 41 | 3.20 | 184 | 0.40 | [15] $^{(b)}$ |
| Co-Ti | 203 | 129 | 68 | 37 | 1.84 | 154 | 0.39 | [25] |

Table 3: Calculated Elastic Properties of Some B1 Transitions Metal Carbides

| System | $c_{11}$ | $c_{12}$ | $c_{44}$ | $C'$ | $A$ | $B$ | $\nu_{100}$ | $\nu_{VR}$ | $G_V$ | $G_R$ | $G_{average}$ | REF |
|---|---|---|---|---|---|---|---|---|---|---|---|---|
| TiC | 513 | 106 | 178 | 204 | 0.87 | 242 | 0.17 | 0.19 | 188 | 187 | 188 | [14] |
| $TiC_{0.91}$ | 515 | 106 | 179 | 205 | 0.88 | 242 | 0.17 | 0.19 | 189 | 188 | 189 | [26] |
| ZrC | 441 | 60 | 151 | 191 | 0.79 | 187 | 0.12 | 0.16 | 167 | 165 | 166 | [14] |
| $ZrC_{0.94}$ | 472 | 99 | 159 | 187 | 0.85 | 223 | 0.17 | 0.20 | 170 | 169 | 169 | [26] |
| $VC_{0.83}$ | 366 | 110 | 192 | 128 | 1.50 | 195 | 0.23 | 0.17 | 166 | 160 | 163 | [14] |
| $VC_{0.84}$ | 501 | 84 | 155 | 209 | 0.74 | 223 | 0.14 | 0.19 | 176 | 173 | 175 | [26] |
| $NbC_{0.9}$ | 413 | 111 | 206 | 151 | 1.36 | 212 | 0.21 | 0.17 | 184 | 180 | 182 | [14] |
| $TaC_{0.90}$ | 505 | 79 | 73 | 213 | 0.34 | 221 | 0.14 | 0.28 | 129 | 99 | 114 | [26, 14] |
| $TaC_{0.97}$ | 610 | 210 | 230 | 200 | 1.15 | 343 | 0.26 | 0.24 | 218 | 217 | 217 | [26] |

#### 4.1.1 Transition-Metal B2 Aluminides and B1 Carbides

The most significant conclusion to be drawn from Table 2 is that there can be significant variations, in both the sign and magnitude of $C'$, even though the predicted variation of $B$ versus $n_e$ is smooth (Figure 13). Values obtained by Voigt-Reuss averaging are clearly invalid when $C'$ becomes negative. In systems where alloying induces a sign change in $C'$, e.g. Al-Nb and Al-V, metastable phases such as the $\omega$ or "O" phase appear on rapid cooling [15]. These metastable phases are related to the high-T stable phases by mechanical instabilities, so they form more easily than stable low-T phases, or assemblages of phases, when cooling is sufficiently rapid. Although it is generally assumed that Poisson's Ratio cannot exceed 0.5, this only holds for mechanically stable phases, and calculated values for $\nu_{100}$ that exceed 0.5 are invariably associated with negative values for $C'$.

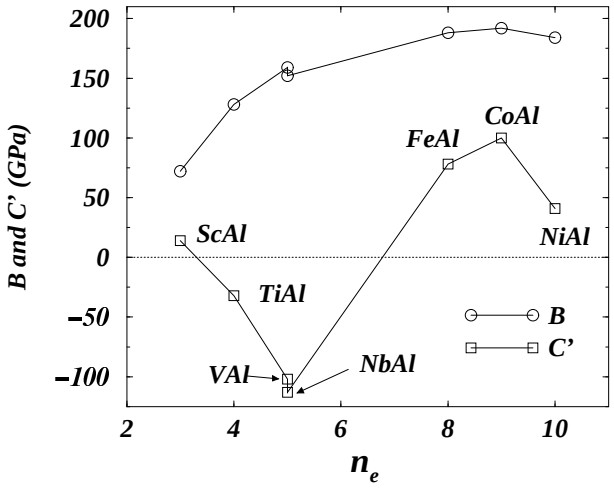


Figure 13: Calculated values of $B$ and $C'$ versus the number of d-electrons $n_e$, for B2 structure transition metal aluminides.

Unlike some of the aluminides in Table 2, the carbides (Table 3) are very stable and do not exhibit negative values for $C'$. It would however be useful to know what happens with isomorphous counter-phases such as FeC. Probably the most significant feature is that the experimental values of $c_{ij}$ appear to be very sensitive to the degree of non-stoichiometry, as do the Debye temperatures [27]. It might be interesting to check what role the elastic constants play in the experimental observation that many of these carbides have their maximum stability away from the stoichiometric composition.

## 4.2 Correlation of Elastic Constants with Melting Temperatures

### 4.2.1 Melting Points

There have been a number of attempts to correlate the melting point $T_m$ with various combinations of elastic constants (Figure 14 [28]). Predictions of melting points from first principles are unreliable, but elastic constants can be calculated by this route. Also, there are known examples of metastable melting points, and it would be useful to estimate the corresponding elastic constants. One of the simplest assumptions is that $T_m$ is proportional to the bulk modulus $B$ (Figure 14a) however this correlation is associated with large error bars so attempts have been made to correlate $T_m$ with other elastic constants. It can be seen from Figure 14b that there is a significant reduction in the scatter when $c_{11}$ is substituted for $B$. This apparently surprising result is understood by combining Eq. 11 and 12 and solving for $c_{11}$:

$$c_{11} = B + 4C'/3 \tag{20}$$

Eq. 20 shows that $c_{11}$ depends upon both $B$, and $C'$ and therefore includes more information about the mechanical stability. As expected, a compound that is approaching a mechanical instability (e.g. $C'>0 \rightarrow 0$ via alloying) typically has a lower $T_m$ than a more stable compound with the same $B$, but a large positive $C'$. Inter-relationships between the various elastic constants allow $c_{11}$ to be expressed as a function of $E$ and $\nu$:

$$c_{11} = E(1-\nu_{100})/((1-2\nu_{100})(1+\nu_{100}) \tag{21}$$

This provides some theoretical justification for a correlation between $T_m$ and $E$ found for silicides [29] and should also work for other structures provided they do not exhibit much variation in $\nu$. This holds for close -packed structures such as A1, A2, A3 (fcc, bcc, HCP) but there are significant variations in $\nu$ when materials of the same structure exhibit a range of ionic or covalent character [30]. Better knowledge of $c_{ij}$ values would allow improved testing of such predictions and should lead to better correlations involving $c_{11}$, $c_{12}$ and $c_{44}$.